



# Effect of synthesis method on structural properties and soot oxidation activity of gadolinium-doped ceria

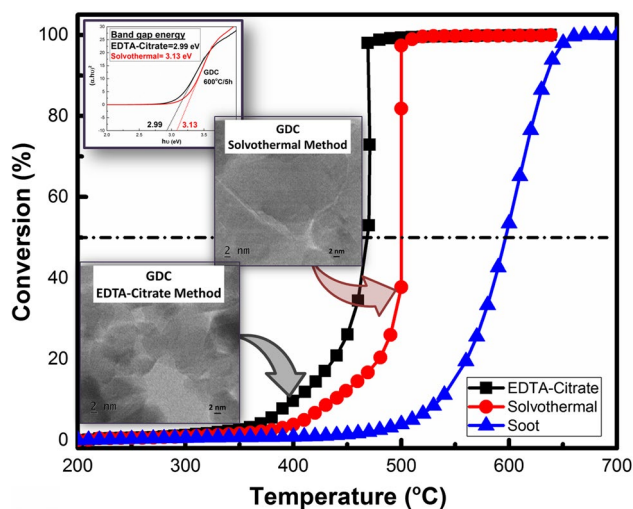
Anjana P. Anantharaman<sup>1</sup> · Hemanth J. Gadiyar<sup>1</sup> · Mythili Surendran<sup>2</sup> · A. Sumadhura Rao<sup>1</sup> · Hari Prasad Dasari<sup>1</sup> · Harshini Dasari<sup>3</sup> · G. Uday Bhaskar Babu<sup>2</sup>

Received: 5 February 2018 / Accepted: 7 June 2018 / Published online: 16 June 2018  
© Institute of Chemistry, Slovak Academy of Sciences 2018

## Abstract

EDTA–citrate complex and solvothermal methods were adopted for the synthesis of gadolinium-doped ceria (GDC) ( $\text{Ce}_{0.9}\text{Gd}_{0.1}\text{O}_2$ ) solid solution, and the obtained GDC sample is tested for soot oxidation activity. Based on XRD results, it was evident that the reactive facet planes of {100} and {110} were highly intense [intensity ratio (%) of (200)/(100) (34.2%) and (220)/(111) (51.2%)] for GDC prepared by the EDTA–citrate method in comparison with the solvothermal method, and this highly intense reactive facet plane correlates to the lower energy for oxygen vacancy formation. Apart from the smaller crystallite size (10 nm) the GDC sample prepared by the EDTA–citrate method displayed lower band gap energy (2.99 eV), higher ratio of reducibility (45.45%) and lower binding energy (528.8 eV) for surface-adsorbed oxygen. The GDC obtained by EDTA–citrate method displayed a better soot oxidation activity ( $T_{50}=468\text{ }^\circ\text{C}$ ) than compared to the GDC obtained by solvothermal method ( $T_{50}=500\text{ }^\circ\text{C}$ ). The obtained results significantly show that the synthesis method plays a crucial role in controlling the structural properties and in enhancing the soot oxidation activity.

## Graphical Abstract



**Keywords** Gadolinium-doped ceria (GDC) · EDTA–citrate complexing method · Solvothermal method · Oxygen vacancy · Soot oxidation activity

**Electronic supplementary material** The online version of this article (<https://doi.org/10.1007/s11696-018-0532-5>) contains supplementary material, which is available to authorized users.

Extended author information available on the last page of the article

## Introduction

Materials of nanosize range with high surface to volume ratio influence the size- and shape-dependent properties along with quantum size effects of electronic features. The catalytic activity of metal oxides has a dependency on its crystal size, crystal surface and exposed crystal planes (Piumetti et al. 2015). The synthesis method holds the key to control the homogeneity of material and thus to maintain a uniform solid solution with better thermal stability (Alifanti et al. 2003). Depending upon the reaction condition undergone during synthesis procedure, particle size, crystal structure and surface area are controlled efficiently along with the specific control over loading of metal on to host lattice (Guillén-hurtado et al. 2015; Mira et al. 2015). The interaction between cations used and hence the redox property of the material is also subjective to the adopted synthesis method (Kozlov et al. 2002). With the variation in synthesis method, crystallite size also varies for CeO<sub>2</sub>-based metal oxides and hence influences on its redox behaviour. Control of surface morphology and size effects by synthesis method modifies active centres for reaction with an improvement in oxygen vacancy (Calvache-Muñoz et al. 2017; Miceli et al. 2015; Zhang et al. 2016). Various synthesis methods are available for synthesis of CeO<sub>2</sub>-based materials, and some of them are hydrolysis (Liu et al. 2010), precipitation (Kuntaiah et al. 2013), sol–gel (Medisetti et al. 2017), hydrothermal (Pan et al. 2008; Piumetti et al. 2015), Glycine–nitrate (Prasad et al. 2010), combustion synthesis (Prasad et al. 2008) and microemulsion method (Malecka et al. 2007).

Synthesis of morphologically modified CeO<sub>2</sub> nanomaterials in different shapes such as nanorods (Zhang et al. 2016; Calvache-Muñoz et al. 2017; Zhang et al. 2016), nanoflakes (Zhang et al. 2016), and nanocubes (Piumetti et al. 2015) is highly adapted. The lower stability of {110} and {100} facet planes in a lattice structure with lower oxygen vacancy formation energy compared to {111} plane can improve redox properties considerably in specific morphologically modified materials (Aneggi et al. 2014). The effect of morphology upon the activity of catalyst studied by Aneggi et al. has proved that the soot oxidation reaction is highly shape dependent in nature. The catalytic activity obtained for pure ceria as nanocubes ( $T_{50}=412$  °C) and nanorods ( $T_{50}=407$  °C) are comparatively higher than conventional polycrystalline ceria ( $T_{50}=447$  °C) samples (Aneggi et al. 2014). Similarly Zhang et al. synthesised ceria nanorods, nanoflakes and nanoparticles and obtained the  $T_{50}$  temperature of 368, 383 and 433 °C, respectively. It is quite evident from the previous studies that the shape control affects the active site and oxygen defect formation of the sample and thus controls the catalytic activity of the sample (Zhang et al. 2016).

Due to thermal and structural instability and redox couple degradation of CeO<sub>2</sub> over an extended operating period, compels to improve its stability by doping with suitable transition metal (Atribak et al. 2008; Piumetti et al. 2016b) or rare earth metal (Bueno-López et al. 2005; Mukherjee et al. 2016) dopant. Dopant addition causes an increase in defect structure that enhances the catalytic activity of the material. Due to the variation in charge and ionic radius between Ce<sup>4+</sup> and Gd<sup>3+</sup>, a considerable alteration in defect structure, oxygen vacancy and oxygen diffusion is resulted (Durgasri et al. 2014). CeO<sub>2</sub>–Gd<sub>2</sub>O<sub>3</sub> binary metal oxides are used in applications such as CO oxidation (Reddy et al. 2016), SOFC electrolyte (Prasad et al. 2008), steam reforming (Prasad et al. 2011), nuclear fuels (Zhu et al. 2010) and so on.

EDTA–citrate method or modified pechini method is a widely adopted technique. During the process, initially, chelation of metal complex ions in solution occurs, further formation of polymeric glass while heating the solution, by a poly-esterification reaction. Sample with molecular level compositional homogeneity and the high surface area at the nanoscale are obtained by this method (Prasad et al. 2012b). On the other hand, there is an improvement in solid solubility in solvothermal synthesis method by maintaining pressure and temperature above its critical point. Hence the reaction between solids will speed up and thus results in homogeneous high pure nanoparticles (Sun et al. 2005). These two synthesis methods are adopted in the current study to analyse in detail the variation in structural properties of the samples due to the changes in reaction conditions. The differences in the synthesis method may lead to differences in the structural properties and thus effect the soot oxidation activity. A fundamental understanding of the effect of synthesis methods on the structural properties will help in fine-tuning of the materials with better catalytic activity.

In the present study, GDC sample is obtained using EDTA–citrate complex and solvothermal methods under fixed-dopant composition (Ce<sub>0.9</sub>Gd<sub>0.1</sub>O<sub>2</sub>) and calcined at 600 °C/5 h. A study on comparison of material properties and their influence on catalytic activity for GDC samples are not yet reported from the author's knowledge. Keeping all other parameters constant and changing only the synthesis method helps in understanding the intrinsic property of the material that varies with respect to the synthesis method. Further, the obtained GDC samples were characterised using XRD, Raman spectroscopy, SEM–EDS, TEM, UV–Vis DRS and XPS analysis. The soot oxidation activity of the GDC samples was tested under tight contact conditions, and effect of synthesis method on structural properties and soot oxidation activity is demonstrated.

## Experimental details

### Synthesis procedure

GDC metal oxide was synthesised using different synthesis methods—EDTA–citrate method and solvothermal method. AR grade chemicals were used for the synthesis method. Solvothermal method (Sun et al. 2005) was used to prepare the GDC sample. In this method, gadolinium chloride hexahydrate ( $\text{GdCl}_3 \cdot 6\text{H}_2\text{O}$ ) (Alfa-Aesar) and cerium chloride heptahydrate ( $\text{CeCl}_3 \cdot 7\text{H}_2\text{O}$ ) (SRL) were used as metal precursor salts. Octadecylamine ( $\text{C}_{18}\text{H}_{39}\text{N}$ ) (SRL), absolute ethanol (99.9%  $\text{C}_2\text{H}_6\text{O}$ ), and ethylenediamine ( $\text{C}_2\text{H}_8\text{N}_2$ ) (Sigma) were other chemicals used for synthesis. A stoichiometric amount of respective metal chloride precursor salts were mixed with 4% octadecylamine dissolved in ethanol solution under continuous stirring condition. Ethylene diamine was added to the obtained solution to control the viscosity and to adjust the pH (9–10). Once the mixture is completely dissolved, the solution was transferred and sealed in a 500 ml Teflon-lined autoclave. A solid solution was obtained by heating the solution in the autoclave at  $150\text{ }^\circ\text{C}/72\text{ h}$ . The solid precursor was calcined at  $600\text{ }^\circ\text{C}/5\text{ h}$ . A small quantity of sample was further calcined at  $900\text{ }^\circ\text{C}/5\text{ h}$  and they were tested for soot oxidation reaction to understand the thermal stability of the samples.

For EDTA–citrate complexing method (Prasad et al. 2012b), cerium nitrate hexahydrate ( $\text{Ce}(\text{NO}_3)_3 \cdot 6\text{H}_2\text{O}$ )  $\geq 99\%$  (SRL chemicals) and gadolinium nitrate hexahydrate ( $\text{Gd}(\text{NO}_3)_3 \cdot 6\text{H}_2\text{O}$ ) 99.9% (Sigma) was used as precursor salts for the synthesis of GDC sample. EDTA (ethylene diamine tetra acetic acid) (SRL chemicals) and citric acid monohydrate (SRL chemicals) were used as chelating agents. Ammonium hydroxide ( $\text{NH}_4\text{OH}$ ) solution (spectrum reagents) is used to adjust the pH and buffering agent. The synthesis procedure is explained in detail elsewhere (Prasad et al. 2012b). After the synthesis, the black precursor salt obtained was oven-dried at  $150\text{ }^\circ\text{C}/24\text{ h}$  and calcined at  $600\text{ }^\circ\text{C}/5\text{ h}$ .

### Characterization

The obtained GDC samples were characterized for X-ray diffraction (XRD) using XPERT Pro diffractometer in the range of  $20^\circ$ – $80^\circ$ , Raman analysis using Bruker RFS 27 spectrometer with 784 nm laser beam, BET surface area and pore volume analysis were measured using SMARTSORB-92/93, scanning electron microscopy (SEM)/energy-dispersive spectroscopy (EDS) using JSM-6380LA, transmission electron microscopy (TEM) using

Joel/JEM 2100, UV–Vis diffusive reflectance spectroscopy (UV–Vis DRS) in a Cary 5000 NIR spectrometer and X-ray photoemission spectroscopy (XPS) using Omicron ESCA + with Al  $\text{K}\alpha$  (1486.6 eV) monochromator. The details of the characterization tools used in the present study is reported in the previous study (Anantharaman et al. 2017).

### Soot oxidation activity measurements

The catalytic activity of the synthesised sample was tested for soot oxidation reaction under tight contact condition in TG/DTA 6300 (Hitachi). Standard soot of Printex-U (Orion Engineered Carbons) was used for the study. The pre-weighed sample mixture of catalyst and soot at a ratio of 4:1 was mixed in a mortar and pestle for 30 min to obtain tight contact sample. Further, the reaction was undergone in TGA with the presence of air at a flow rate of 100 ml/min heating from room temperature to  $600\text{ }^\circ\text{C}$  at a rate of  $10\text{ }^\circ\text{C}/\text{min}$  (Anantharaman et al. 2017). The weight loss was calculated in terms of conversion and plotted with respect to temperature. To check the reproducibility the catalytic activity was measured twice.

## Results and discussion

### XRD analysis

Figure 1 shows GDC sample XRD results synthesised by EDTA–citrate and solvothermal synthesis method, respectively, and Table 1 presents the crystallographic data obtained from its corresponding XRD spectra. The

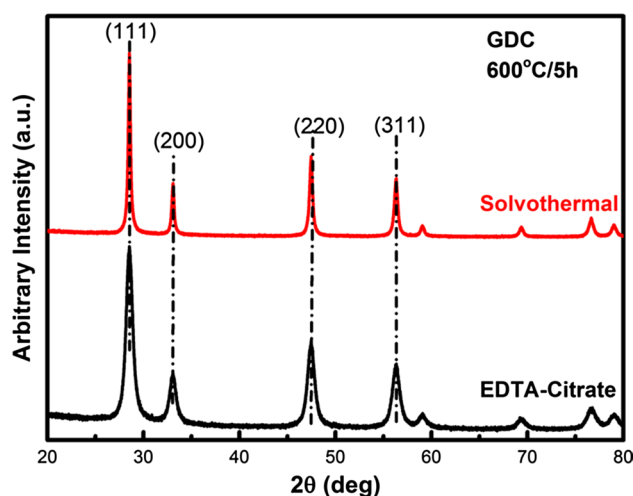


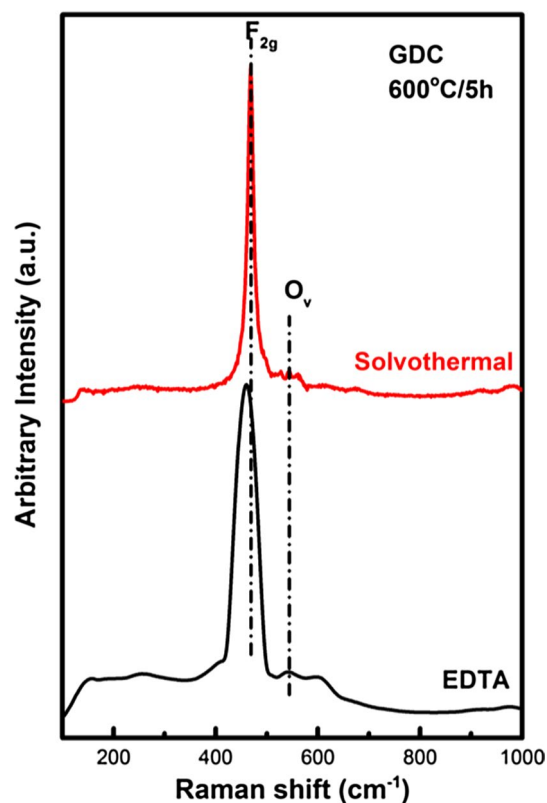
Fig. 1 XRD pattern of GDC samples synthesised by the EDTA–citrate complexing method and solvothermal method calcined at  $600\text{ }^\circ\text{C}/5\text{ h}$

**Table 1** BET surface area, crystallite size, particle size, pore volume, lattice strain and intensity ratios of GDC sample synthesised by different methods

Synthesis method	Crystallite size (nm)	Lattice strain ( $\epsilon$ )	Pore volume ( $\text{cm}^3/\text{g}$ )	Particle size from TEM (nm)	BET surface area ( $\text{m}^2/\text{g}$ )	Intensity ratio (%)	
						(200)/(111)	(220)/(111)
EDTA–citrate	10	0.015	0.0601	10.3	45	34.2	51.2
Solvothermal	24	0.006	0.0530	24.8	43	30.8	45.4

well-resolved peak corresponding to cubic fluorite structure of  $\text{CeO}_2$  without any gadolinium oxide peak confirms the stable solid solution formation in both the samples. Enhanced {100} and {110} facet planes compared to {111} plane lead to improved surface oxygen formation in earlier planes rather than the later. Improved oxygen migration {100} and {110} facet-dominated samples leads to high oxygen mobility (Aneggi et al. 2014). Table 1 provides the intensity ratio of {100}/{111} and {110}/{111} values. It is evident from the result that both {100} and {110} planes are comparatively higher for EDTA–citrate sample rather than the solvothermal sample that may predict the higher reactivity of EDTA–citrate sample due to higher oxygen migration ability (Piumetti et al. 2016a).

Lower crystallite size of the EDTA–citrate sample as shown in Table 1 can lead to better soot–catalyst contact, and thus the intrinsic catalytic activity is expected to improve considerably (Liu et al. 2015). For GDC synthesised by the EDTA–citrate method lattice strain is higher (Table 1), and thus a higher activity for former is expected since the oxygen diffusion is improved (Rushton et al. 2013). Pore volume of the sample may not have significant effect on the activity since the values are considerably lower than the soot size. During the substitution of higher ionic radii dopant on  $\text{CeO}_2$  lattice, lattice deformation is expected that leads to lattice strain which is supposed to cause higher oxygen diffusion, and thus the activity may be enhanced (Rushton et al. 2013). The particle size calculated from the TEM image (see S4 and S5) is given in Table 1 and it shows that the values are almost same as that of the crystallite size of the corresponding samples. The BET surface area of the sample obtained by different synthesis methods are also almost similar (see Table 1). Apart from crystallographic study, the decomposition nature of GDC black precursor before calcination obtained during EDTA–citrate and solvothermal method are analysed using TGA as in (Fig. S1 (a) and (b)). That confirms the complete decomposition of all impurities occur below 600 °C and hence this temperature is used for calcination. Further, surface and bulk phonon information and oxygen availability are obtained from Raman results.

**Fig. 2** Raman spectra of GDC samples synthesised by the EDTA–citrate complexing method and solvothermal method calcined at 600 °C/5 h

### Raman spectroscopy analysis

Figure 2 depicts the Raman spectra of GDC sample synthesised by EDTA–citrate and solvothermal synthesis method. Symmetric breathing of oxygen around ceria atom in cubic fluorite  $\text{CeO}_2$  lattice leads to an intense peak at 460  $\text{cm}^{-1}$  that correspond to triply degenerate  $F_{2g}$  mode (Prasad et al. 2012a). Oxygen vacancy creation due to cation substitution in  $\text{CeO}_2$  lattice while doping influences the width and position of the  $F_{2g}$  peak. Intrinsic and extrinsic oxygen vacancy is evident in both the samples from the peak in spectra at around 540 and 600  $\text{cm}^{-1}$ , respectively (Prasad et al. 2012a). The ratio of the intensity of  $\text{CeO}_2$  peak ( $F_{2g}$ ) to oxygen vacancy peak ( $O_v$ ) provides an idea about the relative oxygen defects available in the system with varying synthesis



**Table 2** Composition, band gap energy, ratio of reducibility,  $O_{\beta}/(O_{\alpha}+O_{\beta}+O_{\gamma})$ ,  $I_{ov}/I_{F2g}$  and  $T_{50}$  of GDC samples synthesised by different methods

Synthesis method	EDS composition (%)		Band gap energy (eV)	Ratio of reducibility (%)	$O_{\beta}$ binding energy (eV)	$I_{ov}/I_{F2g}$	$T_{50}$ (°C)
	Ce	Gd					
EDTA–citrate	89.7	10.3	2.99	45.4	528.8	0.095	468
Solvothermal	90.6	9.4	3.13	31.2	529.1	0.087	500

method (Guo et al. 2011; Sarkar et al. 2017), which is higher for EDTA–citrate complexing method rather than the solvothermal as shown in Table 2. Relative oxygen vacancy concentration and amount of oxygen vacancy follows similar trend as per previous reports (Sarkar et al. 2017). However, the oxygen vacancy concentration calculated based on Raman spectroscopy alone cannot be used to conclude since it considers both surface and bulk oxygen vacancy of the samples. For soot oxidation reaction, specifically, surface oxygen is critical in controlling the activity. Further, XPS analysis will be conducted to understand surface oxygen

vacancy concentration of the samples. To study the morphological variation in the samples with the effect of synthesis method TEM analysis is undergone.

### SEM and TEM analysis

The SEM morphology of GDC sample synthesised by both techniques (Fig. S2 (a) and (b)) confirms the similar structure in both the cases. The atomic composition obtained from EDS for GDC synthesised by both methods are shown in Table 2. The compositions calculated are similar to the

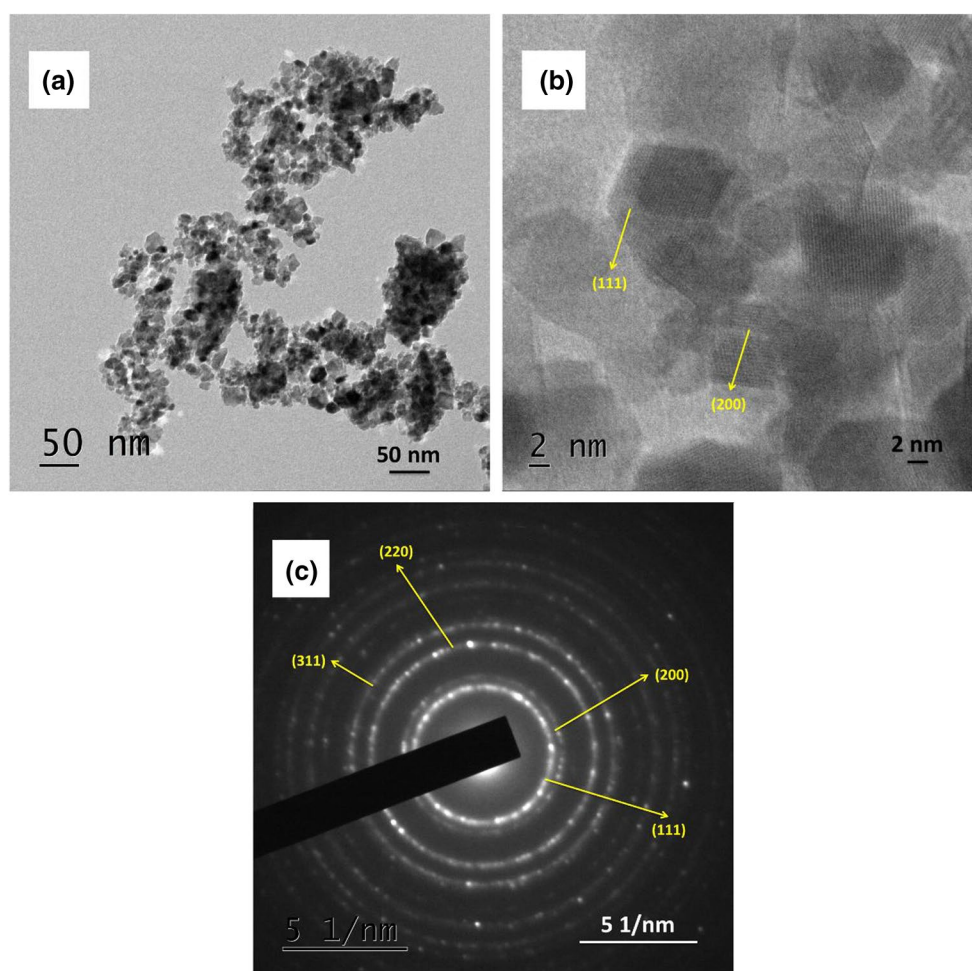


**Fig. 3** **a** TEM image, **b** HR-TEM image and **c** SAED pattern of GDC sample synthesised by EDTA–citrate complexing method calcined at 600 °C/5 h

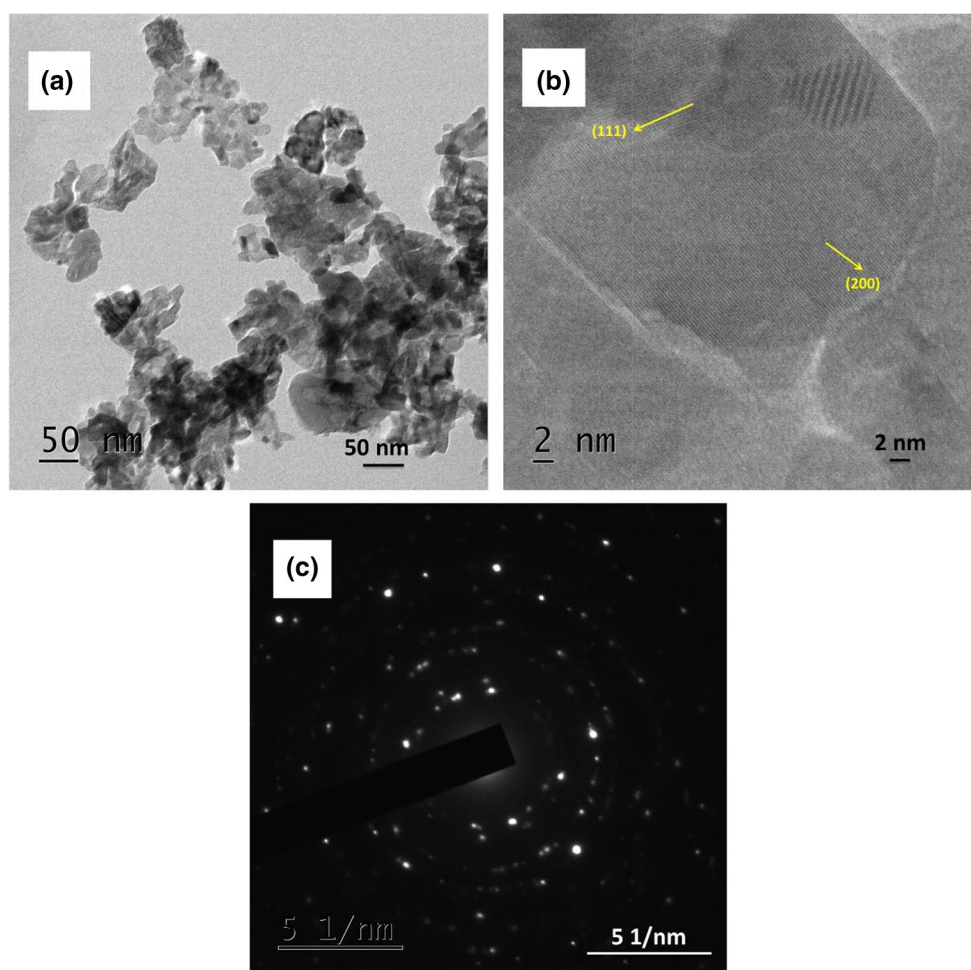
theoretical composition ( $\text{Ce}_{0.9}\text{Gd}_{0.1}\text{O}_2$ ) due to homogeneous mixing during both synthesis methods. Structural evaluation at the atomic scale is undergone using TEM analysis for GDC samples synthesised by EDTA–citrate and solvothermal synthesis method. Figures 3 and 4 depicts the TEM images obtained during EDTA–citrate and solvothermal synthesis method, respectively. The TEM image of EDTA–citrate sample shown in Fig. 3a confirms that the particles are almost spherical. Planes corresponding to (111) and (200) are identified from the fringes of the HR-TEM image (Fig. 3b). The Debye characteristic rings in SAED pattern as shown in Fig. 3c confirms the polycrystalline nature of the sample. Each ring in the SAED is indexed corresponding to each plane, which matches very well with the planes calculated from XRD result. Similarly, the TEM image (see Fig. 4a) of GDC sample synthesised by solvothermal method confirms that particles are aggregated without any specific shape. The morphology obtained for each synthesis methods are different in nature as evident from their corresponding TEM images. The HR-TEM image in Fig. 4b shows lattice fringes corresponding to (111) and (200) plane as evident in XRD result of the sample. The appearance of Bragg spots

from SAED pattern shown in Fig. 4c confirms the larger size of crystals obtained when compared to sample obtained from EDTA–citrate method. The crystallite size obtained from XRD also shows that solvothermal sample has higher crystallite size than EDTA–citrate sample. Further, the variation in sample coordination and the band gap is studied using UV–Vis DRS analysis on both the samples.

### UV–Vis DRS analysis

Figure 5a shows the UV–Vis DRS of GDC sample synthesised by EDTA–citrate and solvothermal synthesis techniques. GDC synthesised by both method shows a sharp absorption band below 400 nm. Two absorption spectra around 270 and 330 nm which corresponds to  $\text{O}^{2-} \rightarrow \text{Ce}^{4+}$  charge transaction and inter-band transaction of  $\text{CeO}_2$ , respectively, is evident in both the samples (Prasad et al. 2012a). The absorption intensity is higher for GDC sample synthesised by solvothermal method than that of the EDTA–citrate method. Figure 5b depicts the band gap energy calculated using Tauc's plot. The value of band gap energy given in Table 2 confirms that the lower band gap

**Fig. 4** a TEM image, b HR-TEM image and c SAED pattern of GDC sample synthesised by solvothermal method calcined at 600 °C/5 h



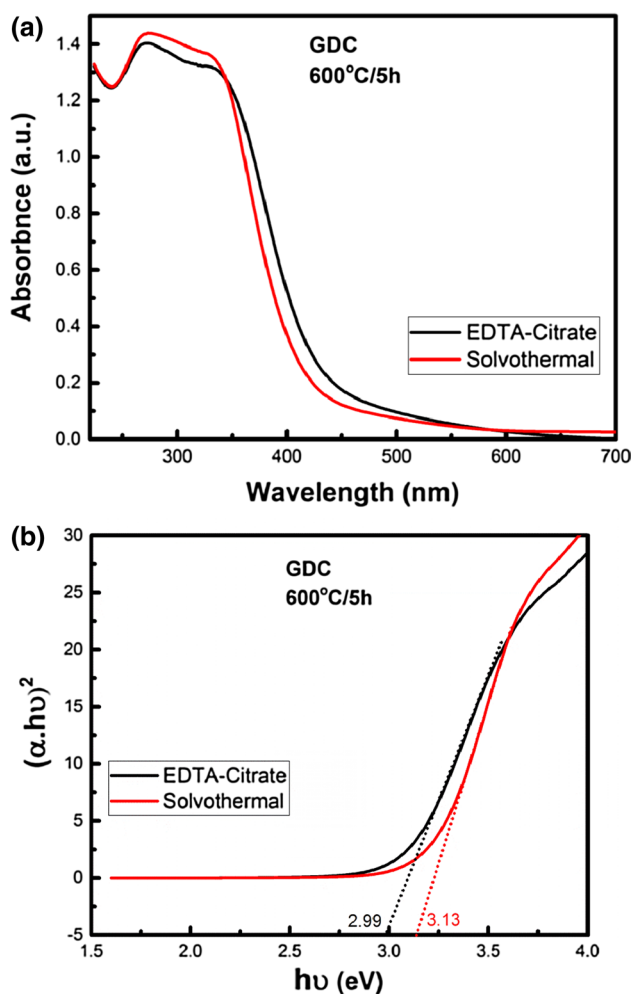


**Fig. 5** **a** UV–Vis DRS plot and **b** Tauc's plot of GDC samples synthesised by the EDTA–citrate complexing method and solvothermal method calcined at 600 °C/5 h

energy is obtained for EDTA–citrate sample in comparison with the solvothermal sample. The oxygen vacancy formation energy can be directly correlated to the band gap energy since it is the energy required for transfer of electrons from highest filled (O 2p) to lowest filled (Ce 4f) orbitals. With a reduction in the band gap energy, oxygen available for the reaction will also improve correspondingly (Getsoian et al. 2014). Thus, based on the band gap energy, the energy for oxygen vacancy formation is expected to be lower for EDTA–citrate-synthesised GDC rather than the solvothermal method, and this may affect in enhancing the activity of GDC synthesised by the EDTA–citrate method.

### XPS analysis

Multiple oxidation state and oxygen vacancy of the sample is analysed using XPS analysis. The XPS spectra of GDC samples obtained from the two synthesis methods are

depicted in Fig. 6. Figure 6a and b illustrate Ce 3d and O 1s spectra of XPS analysis, respectively. The Ce 3d core-level spectrum shows seven peaks corresponding to Ce<sup>3+</sup> ( $v_0$ ,  $u_0$  and  $v'$ ) and Ce<sup>4+</sup> ( $v$ ,  $v''$ ,  $v'''$  and  $u''$ ) oxidation state over the surface of CeO<sub>2</sub> (Prasad et al. 2012a). The presence of Ce<sup>3+</sup> confirms the availability of oxygen vacancy and is in a partially reduced form. The ratio of reducibility (Ce<sup>3+</sup>/Ce<sup>3+</sup>+Ce<sup>4+</sup>) is calculated from the Ce 3d XPS plot and given in Table 2. EDTA–citrate sample has a higher ratio of reducibility which implies an easy reduction of the sample and thus higher oxygen vacancy rather than solvothermal sample (Zhang et al. 2016). Three peaks obtained from O 1s XPS in Fig. 6b is apparent for the existence of lattice oxygen (O<sub>α</sub>), surface adsorbed oxygen (O<sub>β</sub>) and oxygen in carbonates and hydroxide (O<sub>γ</sub>) (Prasad et al. 2012a). The catalyst to soot active oxygen transfer may be enhanced by surface-adsorbed oxygen presence as per previous results (Zhang et al. 2016). For the catalyst with easy removal of surface oxygen, the catalytic oxidation activity is improved further. Thus, lowering of binding energy is directly correlated to the easy removal of surface oxygen, which can hence enhance the catalytic reaction. Table 2 shows binding energy values of surface oxygen for both the samples. The value confirms that the amount of fast release of surface oxygen in GDC sample synthesised by EDTA–citrate is higher than that by the solvothermal method. The Gd 3d spectra are analysed and confirm that the single oxidation state of Gd<sup>3+</sup> is obtained in both the samples. Based on all the characterisation techniques utilised, it can be concluded that GDC obtained using EDTA–citrate method might be possibly having a higher catalytic soot oxidation activity rather than the solvothermal sample. Soot activity is further analysed for both the samples.

### Soot oxidation activity

The soot oxidation catalytic activity of GDC samples synthesised by EDTA–citrate and solvothermal synthesis under tight contact condition is as illustrated in Fig. 7. Table 2 represents the  $T_{50}$  temperature obtained for both the samples. Different steps involved in the soot oxidation mechanism are oxygen adsorption, oxygen spillover to active carbon sites, surface oxygen complexes (SOC) formation by active carbon chemisorption and SOC desorption. The primary step involving soot oxidation reaction is the spillover of oxygen onto active carbon sites and their chemisorption subsequently. Soot oxidation reaction occurs at the interface of soot and catalyst surface (Prasad et al. 2012b). The spillover mechanism can be related to the ease of active oxygen formation, oxygen mobility within the lattice and redox sites (Sudarsanam et al. 2015). GDC sample synthesised by EDTA–citrate complexing method showed considerably

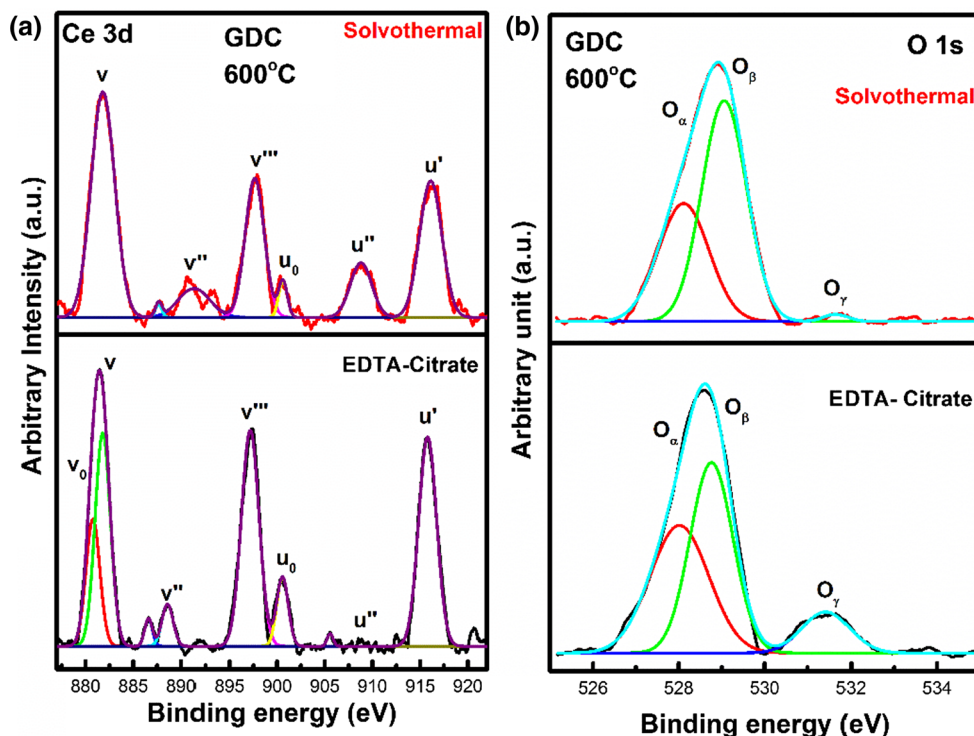


**Fig. 6** XPS of **a** Ce 3d and **b** O 1s of GDC samples synthesised by the EDTA–citrate complexing method and solvothermal method calcined at 600 °C/5 h

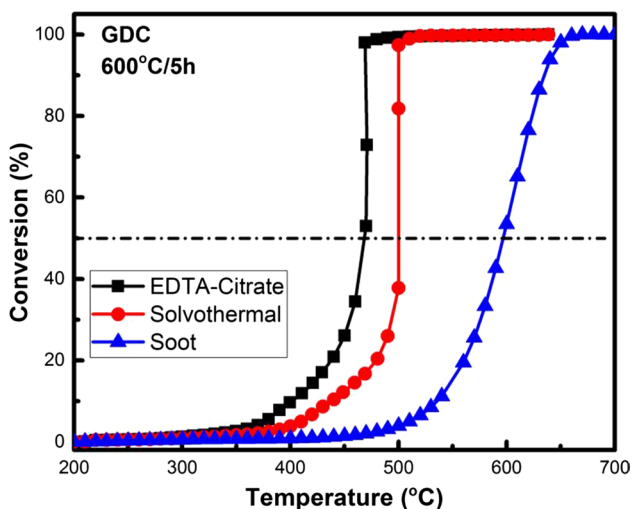


**Fig. 7** Soot oxidation of plane soot sample, GDC samples synthesised by the EDTA–citrate complexing method and solvothermal method calcined at 600 °C/5 h

lower oxidation temperature ( $T_{50}=468$  °C) than the solvothermal sample ( $T_{50}=500$  °C).

Durgasri et al. (Durgasri et al. 2014) have studied the soot oxidation activity of  $\text{Ce}_{0.8}\text{Gd}_{0.2}\text{O}_{2.8}$  (calcined at 500 °C) synthesised by modified coprecipitation method and obtained

a  $T_{50}$  temperature of 472 °C (Durgasri et al. 2014). Even though the TEM morphology remains the same, the BET surface area ( $74 \text{ m}^2/\text{g}$ ) obtained by the reported study is considerably higher than both the samples obtained in this study. The variation in structural parameters and catalytic activity could be due to the difference in composition, synthesis method and calcination temperature (Durgasri et al. 2014).  $\text{CeO}_2\text{--ZrO}_2$  sample synthesised by Aneggi et al. (Aneggi et al. 2012) calcined at 600 °C resulted in a  $T_{50}$  temperature of 390 °C which is significantly lower values compared to the values obtained for GDC in the current study. The higher catalytic activity of the sample is pointed out due to the availability of more reactive facet planes of (110) and (100) (Aneggi et al. 2012). The synthesis method adopted in this study varies from the literature reported, that results in modification of more reactive planes compared and affects the catalytic activity. The  $\text{CO}_2$  selectivity of  $\text{CeO}_2$ -based catalyst is considerably higher under tight contact condition due to relatively slow oxidation process as reported by previous literatures confirms the same for GDC samples obtained in the present study (Reddy and Rao 2009; Wu et al. 2007; Zamar et al. 1995).

Based on the primary characterisation studies undergone, it can be concluded that the textural and structural property of catalyst plays a crucial role in controlling its activity. Highly reactive and low energy indexed {100}, and {110} facets



in GDC sample synthesised by EDTA–citrate complexing method, as per XRD and TEM analysis, leads to higher catalytic activity due to lower energy for oxygen vacancy formation in this planes (Aneggi et al. 2012). Contact points between soot and catalyst can be improved by decreasing crystallite size and increasing pore volume of catalyst (Durgasri et al. 2014; Miceli et al. 2015). Improved lattice strain can enhance the oxygen diffusion into the lattice and thus aids in improved oxygen mobility which influences the activity of the catalyst positively (Rushton et al. 2013). Smaller crystallite size, larger pore volume and higher lattice strain value obtained for GDC sample synthesised by EDTA–citrate method has improved catalytic activity due to enhanced contact points and oxygen mobility when compared to sample prepared by solvothermal method as per this study. The lower band gap energy of EDTA–citrate sample confirms the lower energy for oxygen vacancy formation and thus aids in catalytic activity of the sample (Getsoian et al. 2014). The binding energy of surface oxygen is the lowest in case of GDC samples obtained by EDTA–citrate method that proves the easy removal of surface oxygen for soot oxidation reaction and thus can enhance the activity (Mukherjee et al. 2016). Surface active sites with better redox potential to shift from  $\text{Ce}^{3+}/\text{Ce}^{4+}$  is a critical parameter that controls the activity of catalyst (Durgasri et al. 2014). In conclusion, the EDTA–citrate GDC sample with higher reactive facet planes, smaller crystallite size, higher lattice strain, lower band gap energy, surface-adsorbed oxygen with lower-binding energy, higher reducibility of  $\text{Ce}^{4+}$  to  $\text{Ce}^{3+}$  results in enhancing the soot activity by improving contact points and oxygen mobility. It is not a single parameter that controls the activity of catalyst for soot oxidation, instead the intrinsic (oxygen availability) and extrinsic (surface contact points) property controls together simultaneously.

## Conclusion

GDC solid solution was synthesised using solvothermal and EDTA–citrate complexing methods. XRD results confirm the crystal planes, crystal structure, lattice strain, lattice parameter and crystallite size. The intensity ratio of different planes was calculated, and the lower energy facet planes of {100} and {110} are highly intense for EDTA–citrate sample. Apart from that, smaller crystallite size (10 nm), higher lattice strain (0.015) and higher pore volume ( $0.0601 \text{ cm}^3/\text{g}$ ) were observed for EDTA–citrate sample. The superior soot oxidation activity of GDC prepared of the EDTA–citrate method is due to its low-binding energy of surface oxygen and high  $\text{Ce}^{3+}/\text{Ce}^{4+}$  redox cycle (XPS) analysis, and a low band gap energy (UV–Vis DRS analysis). The result obtained from the current study were in favour for the EDTA–citrate method, and thus it has a better catalytic activity ( $T_{50}=468 \text{ }^\circ\text{C}$ ) rather than solvothermal synthesis method ( $T_{50}=500 \text{ }^\circ\text{C}$ ). The EDTA–citrate complexing method is possibly a potential synthesis technique

that can be adopted for the synthesis of catalytic materials with comparatively better catalytic properties.

**Acknowledgements** This work is funded by DST-Inspire Faculty Award (IFA-13 ENG-48). Thanks to MRC, MNIT Jaipur for facilitating Raman and XPS data. We acknowledge SAIF STIC, Cochin for UV–Vis DRS and TEM data. We would like to thank Department of Metallurgy and Material Science Engineering and Department of Chemistry for providing SEM and FTIR data, respectively.

**Author contributions** APA, HJG, MS and SRA obtained the experimental data. XRD and BET surface area data are provided by UBB and HD, respectively. HPD conceived the study. APA, HJG and HPD analysed all the experimental data. Writing and document editing was contributed by all authors.

## References

- Alifanti M, Baps B, Blangenois N, Naud J, Grange P, Delmon B (2003) Characterization of  $\text{CeO}_2\text{-ZrO}_2$  mixed oxides. Comparison of the citrate and sol–gel preparation methods. *Chem Mater* 15(2):395–403
- Anantharaman AP, Dasari HP, Lee J-H, Dasari H, Babu GUB (2017) Soot oxidation activity of redox and non-redox metal oxides synthesised by EDTA–citrate method. *Catal Lett* 147(12):3004–3016
- Aneggi E, de Leitenburg C, Llorca J, Trovarelli A (2012) Higher activity of diesel soot oxidation over polycrystalline ceria and ceria–zirconia solid solutions from more reactive surface planes. *Catal Today* 197(1):119–126
- Aneggi E, Wiater D, de Leitenburg C, Llorca J, Trovarelli A (2014) Shape-dependent activity of ceria in soot combustion. *ACS Catal* 4(1):172–181
- Atribak I, Bueno-López A, García-García A (2008) Thermally stable ceria–zirconia catalysts for soot oxidation by  $\text{O}_2$ . *Catal Commun* 9(2):250–255
- Bueno-López A, Krishna K, Makkee M, Moulijn JA (2005) Enhanced soot oxidation by lattice oxygen via  $\text{La}^{3+}$ -doped  $\text{CeO}_2$ . *J Catal* 230(1):237–248
- Calvache-Muñoz J, Prado FA, Rodríguez-Páez JE (2017) Cerium oxide nanoparticles: synthesis, characterization and tentative mechanism of particle formation. *Colloids Surf A Physicochem Eng Asp* 529(May):146–159
- Durgasri DN, Vinodkumar T, Reddy BM (2014) Facile synthesis of catalytically active  $\text{CeO}_2\text{-Gd}_2\text{O}_3$  solid solutions for soot oxidation. *J Chem Sci Indian Acad Sci* 126(2):429–435
- Getsoian AB, Zhai Z, Bell AT (2014) Band-gap energy as a descriptor of catalytic activity for propene oxidation over mixed metal oxide catalysts. *J Am Chem Soc* 136:13684–13697
- Guillén-hurtado N, García-garcía A, Bueno-lópez A (2015) Active oxygen by Ce–Pr mixed oxide nanoparticles outperform diesel soot combustion Pt catalysts. *Appl Catal B Environ* 174–175(2):60–66
- Guo M, Lu J, Wu Y, Wang Y, Luo M (2011) UV and visible Raman studies of oxygen vacancies in rare-earth-doped ceria. *Langmuir* 27(7):3872–3877
- Kozlov AI, Kim DH, Yezerets A, Andersen P, Kung HH, Kung MC (2002) Effect of preparation method and redox treatment on the reducibility and structure of supported ceria–zirconia mixed oxide. *J Catal* 209:417–426

- Kuntaiah K, Sudarsanam P, Reddy BM, Vinu A (2013) Nanocrystalline  $Ce_{1-x}Sm_xO_{2-8}$  ( $x=0.4$ ) solid solutions: structural characterization versus CO oxidation. *RSC Adv* 3(21):7953
- Liu J, Zhao Z, Xu C, Duan A, Jiang G (2010)  $CeO_2$ -supported vanadium oxide catalysts for soot oxidation: the roles of molecular structure and nanometer effect. *J Rare Earths* 28(2):198–204
- Liu S, Wu X, Weng D, Ran R (2015) Ceria-based catalysts for soot oxidation: a review. *J Rare Earths* 33(6):567
- Małecka MA, Kępiński L, Miśta W (2007) Structure evolution of nanocrystalline  $CeO_2$  and  $CeLnOx$  mixed oxides ( $Ln=Pr, Tb, Lu$ ) in  $O_2$  and  $H_2$  atmosphere and their catalytic activity in soot combustion. *Appl Catal B Environ* 74(3–4):290–298
- Mediseti S, Ahn J, Patil S, Goel A, Bangaru Y (2017) Synthesis of GDC electrolyte material for IT-SOFCs using glucose and fructose and its characterization. *Nano Struct Nano Objects* 11:7–12
- Miceli P, Bensaïd S, Russo N, Fino D (2015) Effect of the morphological and surface properties of  $CeO_2$ -based catalysts on the soot oxidation activity. *Chem Eng J* 278:190–198
- Mira JG, Pérez VR, Bueno-lópez A (2015) Effect of the CeZrNd mixed oxide synthesis method in the catalytic combustion of soot. *Catal Today* 253:77–82
- Mukherjee D, Rao BG, Reddy BM (2016) CO and soot oxidation activity of doped ceria: influence of dopants. *Appl Catal B Environ* 197:105–115
- Pan C, Zhang D, Shi L, Fang J (2008) CTAB assisted hydrothermal synthesis, controlled conversion, and CO oxidation properties of  $CeO_2$  nanorods, nanotubes, nanowires, and nanocubes. *Eur J Inorg Chem* 181(15):2429–2436
- Piumetti M, Bensaïd S, Russo N, Fino D (2015) Nanostructured ceria-based catalysts for soot combustion: investigations on the surface sensitivity. *Appl Catal B Environ* 165:742–751
- Piumetti M, Andana T, Bensaïd S, Russo N, Fino D, Pirone R (2016a) Study on the CO oxidation over ceria-based nanocatalysts. *Nanoscale Res Lett* 11(165):1–8
- Piumetti M, Bensaïd S, Russo N, Fino D (2016b) Investigations into nanostructured ceria-zirconia catalysts for soot combustion. *Appl Catal B Environ* 180:271–282
- Prasad DH, Son JW, Kim BK, Lee HW, Lee JH (2008) Synthesis of nano-crystalline  $Ce_{0.9}Gd_{0.1}O_{1.95}$  electrolyte by novel sol-gel thermolysis process for IT-SOFCs. *J Eur Ceram Soc* 28(16):3107–3112
- Prasad HD, Son J, Kim B, Lee H, Lee J (2010) A significant enhancement in sintering activity of nanocrystalline  $Ce_{0.9}Gd_{0.1}O_{1.95}$  powder synthesized by a glycine-nitrate-process. *Ceram Process Res* 11(2):176–183
- Prasad DH, Ji H, Kim H, Son J, Kim B, Lee H, Lee J (2011) Effect of nickel nano-particle sintering on methane reforming activity of Ni-CGO cermet anodes for internal steam reforming SOFCs. *Appl Catal B Environ* 101:531–539
- Prasad DH, Park SY, Ji HI, Kim HR, Son JW, Kim BK, Lee HW, Lee JH (2012a) Structural characterization and catalytic activity of  $Ce_{0.65}Zr_{0.25}RE_{0.1}O_{2-8}$  nanocrystalline powders synthesized by the glycine-nitrate process. *J Phys Chem C* 116(5):3467–3476
- Prasad DH, Park SY, Oh EO, Ji H, Kim HR, Yoon KJ, Son JW, Lee JH (2012b) Synthesis of nano-crystalline  $La_{1-x}Sr_xCoO_{3-8}$  perovskite oxides by EDTA-citrate complexing process and its catalytic activity for soot oxidation. *Appl Catal A Gen* 447–448:100–106
- Reddy BM, Rao KN (2009) Copper promoted ceria-zirconia based bimetallic catalysts for low temperature soot oxidation. *Catal Commun* 10:1350–1353
- Reddy BM, Vinodkumar T, Durgasr Naga D, Rangaswamy A (2016) Synthesis and characterization of nanostructured  $Ce_{0.8}M_{0.2}O_{2-8}$  ( $M=Sm, Eu, and Gd$ ) solid solutions for catalytic CO oxidation. *Proc Natl Acad Sci India Sect A Phys Sci* 87(1):155–161
- Rushton MJD, Chroneos A, Skinner SJ, Kilner JA, Grimes RW (2013) Effect of strain on the oxygen diffusion in yttria and gadolinia co-doped ceria. *Solid State Ion* 230:37–42
- Sarkar A, Loho C, Velasco L, Thomas T, Bhattacharya SS, Hahn H, Djenadic RR (2017) Multicomponent equiatomic rare earth oxides with narrow band gap and associated praseodymium multivalency. *Dalt Trans* 46:12167–12176
- Sudarsanam P, Hillary B, Deepa D, Amin MH, Malleshram B, Reddy BM, Bhargava SK (2015) Highly efficient cerium dioxide nanocubes-based catalyst for low temperature diesel soot oxidation: cooperative effect of cerium- and cobalt-oxides. *Catal Sci Technol* 5:3496–3500
- Sun C, Li H, Zhang H, Wang Z, Chen L (2005) Controlled synthesis of  $CeO_2$  nanorods by a solvothermal method. *Nanotechnology* 16:1454–1463
- Wu X, Liang Q, Weng D, Lu Z (2007) The catalytic activity of  $CuO-CeO_2$  mixed oxides for diesel soot oxidation with a  $NO/O_2$  mixture. *Catal Commun* 8(12):2110–2114
- Zamar F, Trovarelli A, de Leitenburg C, Dolcetti G (1995)  $CeO_2$ -based solid solutions with the fluorite structure as novel and effective catalysts for methane combustion. *J Chem Soc Chem Commun* 2:965
- Zhang W, Niu X, Chen L, Yuan F, Zhu Y (2016) Soot combustion over nanostructured ceria with different morphologies. *Sci Rep* 6:1–10
- Zhu B, Tahara Y, Yasunaga K, Matsui T, Hori F, Iwase A (2010) Study on analysis of crystal structure in  $CeO_2$ -doped with  $Er_2O_3$  or  $Gd_2O_3$ . *J Rare Earths* 28(SUPPL. 1):164–167

## Affiliations

Anjana P. Anantharaman<sup>1</sup> · Hemanth J. Gadiyar<sup>1</sup> · Mythili Surendran<sup>2</sup> · A. Sumadhura Rao<sup>1</sup> · Hari Prasad Dasari<sup>1</sup> · Harshini Dasari<sup>3</sup> · G. Uday Bhaskar Babu<sup>2</sup>

✉ Hari Prasad Dasari  
energyhari@nitk.edu.in

<sup>1</sup> Chemical Engineering Department, National Institute of Technology Karnataka, Mangalore 575025, India

<sup>2</sup> Chemical Engineering Department, National Institute of Technology Warangal, Warangal 506004, India

<sup>3</sup> Chemical Engineering Department, Manipal Institute of Technology, Manipal Academy of Higher Education, Manipal 576104, India